Asphaltene Molecular Size and Structure

Henning Groenzin and Oliver C. Mullins*

Schlumberger-Doll Research, Ridgefield, Connecticut 06877

Received: July 27, 1999

The rotational correlation times of individual asphaltene molecules have been determined using fluorescence depolarization techniques, addressing an active, long-standing controversy. Using simple theoretical models and using model-independent comparisons with known chromophores, a range of asphaltene molecular diameters is obtained of 10−20 Å. Comparison with corresponding data of known chromophores indicates a molecular mass for asphaltene molecules of 500−1000 amu. Furthermore, we have performed the first direct measurement correlating molecular size with constituent chromophore size; we establish that the bulk of asphaltene molecules possess 1 or 2 (aromatic) chromophores per molecule. Similar results are found for the largest aromatic molecules of the de-asphaltened crude oil.

I. Introduction

Petroleum asphaltenes are the heaviest, most aromatic component of crude oil. Asphaltene, a complex molecular mixture, is a friable, infusible solid that is colloidally dispersed in crude oil representing a mass fraction of 0−10% or more.[1−6] Asphaltenes are defined in terms of a solubility classification, not by chemical structure, in part due to the convenient methods employed to isolate asphaltenes from crude oil and in part due to the difficulty of completely defining asphaltene molecular properties. A common but not unique definition of petroleum asphaltenes is: they are the petroleum component that is insoluble in *n*-heptane and soluble in toluene. This widely used definition is the one we employ. Other definitions employ a different precipitating solvent, such as *n*-hexane or *n*-pentane, yielding a somewhat different petroleum fraction. In any event, the solubility classification isolates the heaviest, most aromatic portion of crude oil; thus, this classification is extremely useful.

Asphaltenes are of concern due to their enormous impact on several utilitarian processes and materials. Crude oil production, transportation, and refining are all strongly affected by the asphaltene contained in the crude oil.[1−6] Generally, asphaltenes increase the difficulties of crude oil utilization, an issue of growing importance as low-asphaltene crude oils are preferentially consumed, leaving the asphaltic oils to be utilized. The asphaltene content of paving tar and of asphaltic coating materials strongly affects rheological and adhesive properties and, as such, is of extreme economic value.[1−6]

Even though asphaltenes are defined in terms of a solubility class, asphaltenes, particularly from one source such as unrefined crude oil, are found to exhibit rather uniform chemical properties. Many bulk properties of asphaltenes have been extensively studied, revealing much about their molecular structure and aggregation propensities. For example, asphaltenes are predominantly carbon and hydrogen with a C:H atomic ratio near 1:1.1. ^{13}C NMR shows that ~40% of the carbon is aromatic.[3,6,7] ^{1}H NMR and IR show that ~90% of the hydrogen is substituted on saturated carbon, primarily in methylene and some methyl groups.[3,6,7] Asphaltenes also possess heteroatoms at the several mass percent level. XANES[8,9] and XPS[10] spectroscopy show

that asphaltene sulfur is found in thiophene and sulfide and a little in sulfoxide.[5,9] XANES was also used to show that asphaltene nitrogen is all in aromatic rings, both pyrrolic (dominant) and pyridinic.[5,11] X-ray,[12] neutron,[13−15] and optical[16] scattering methods have been very effective in uncovering the systematics of aggregation properties of asphaltenes. The diameter of the asphaltene micelles is approximately 60 Å;[1−6] molecular modeling supports the contention that the fundamental micelle is unable to grow larger due to steric interactions.[14] The fact that petroleum asphaltenes exhibit many well behaved chemical regularities justifies the chemical characterization of this solubility class, the asphaltenes.

In spite of the wealth of information about asphaltenes, several fundamental properties are not known. In particular, divergent measurements on the molecular weight have persisted for 20 years, with discrepancies being on the order of a factor of 10. In addition, there has been no direct measurement of the number of fused aromatic ring systems per asphaltene molecule; estimates have ranged from 1 to 20. Such large disagreements are simply unacceptable, these issues must be resolved. Colligative methods such as vapor pressure osmometry (VPO) have been used to measure asphaltene molecular weights, yielding values of several thousand amu.[1−6,17−19] Size exclusion chromatography (or gel permeation chromatography (GPC)) yields even larger values, nearly 10 000 amu.[19] However, the high concentration of asphaltenes in solution needed to observe an effect yields aggregates or micelles of asphaltenes, not individual molecules, giving rather large estimations of asphaltene molecular weights.[17−19] The aggregation properties of asphaltenes are well-known,[1−6] and critical micelle concentrations for asphaltenes have been determined.[18,19] It is clear that the VPO technique suffers from the aggregation problem. GPC has been used to estimate asphaltene molecular size and, by comparison with known standards, molecular weight. However, concentrations in excess of the critical micelle concentration have been used. Furthermore, significant uncertainty exists when comparing the interaction of asphaltenes versus polystyrene standards with the GPC matrix, compounding the difficulty of determining asphaltene molecular weight with GPC.[20]

The application of field ionization mass spectroscopy (FIMS) on asphaltenes indicates that molecular weights of asphaltenes

are on the order of 800 amu.[21,22] More recently, laser desorption mass spectroscopy (LDMS) has also been used to measure asphaltene molecular weights.[23] These asphaltenes, prepared from resid, were found to have a molecular weight of around 400 amu.[23] An extensive effort was undertaken to rule out fragmentation and to prove that the heavier asphaltenes were being volatilized. Nevertheless, these two issues, along with conflicting measurements of much larger molecular weights from other techniques, have helped sustain the controversy regarding asphaltene molecular weights.

In addition to the controversy regarding the molecular weights, there has been considerable uncertainty about the number of fused aromatic rings in the asphaltene moieties. There has been no direct measurement of the number of fused-ring systems per asphaltene molecule. Mass spectroscopy results were used to measure the number of aromatic rings per molecule, but these results are unable to distinguish fused- from separate-ring systems.[23]

Another key issue of asphaltene molecular structure is the number of rings per fused-ring system (or aromatic moiety). Estimates of the dominant number of rings fused in asphaltene aromatic moieties have ranged from 4 to 20.[1-6] The larger numbers for fused rings are incompatible with smaller molecular weights. Various techniques suggest that the average number of rings fused in asphaltene aromatic moieties is less than 10; these techniques include X-ray scattering,[1-3,12] NMR,[1-3,5,7] optical absorption,[24-26] and fluorescence emission spectroscopy.[24,27] Scanning tunneling microscopy (STM) has been used to image directly the aromatic (conductive) components of asphaltene molecules.[28] Size estimates of the fused aromatic ring moieties from these images are approximately 10 Å, with six rings fused in a chromophore being particularly evident. The convergence of results from these many techniques has led to the general acceptance that asphaltene aromatic moieties contain 4–10 fused rings.[6]

Consequently, if larger asphaltene molecular weights are correct, then there must be many fused aromatic moieties per asphaltene molecule. A recently proposed asphaltene molecular structure which is often cited contains 18 separate (but covalently linked) aromatic ring systems along with a large molecular weight (>6000 amu).[29] As these authors point out, if asphaltenes actually possess smaller molecular weights, then they would propose the same molecular groups, but not covalently linked. With the generally accepted view that fused aromatic moieties are not so large, the debate on asphaltene molecular weights essentially reduces to whether individual aromatic asphaltene moieties are covalently linked to each other via saturated bridges or whether aromatic moieties are bonded via van der Waals interactions, dipole-dipole interactions, and other noncovalent bonding.

Here, we analyze the fluorescence depolarization rates of very dilute solutions of asphaltenes. These rates are related directly to molecular size with robust, widely used models. In addition, we analyze known chromophores to provide a model-independent analysis of these results. These known chromophores allow direct estimation of asphaltene molecular sizes. Furthermore, the known dependence of chromophore size to spectral properties has allowed us to correlate the rotation rate of chromophores imbedded in asphaltene molecules with the rotation rate of the molecule as a whole. The excellent correlation of chromophore size to total molecular size over a very broad range strongly implies that asphaltene molecules have one or two fused-ring systems per molecule. This is the first direct correlation of asphaltene chromophore size to molecular size. The largest
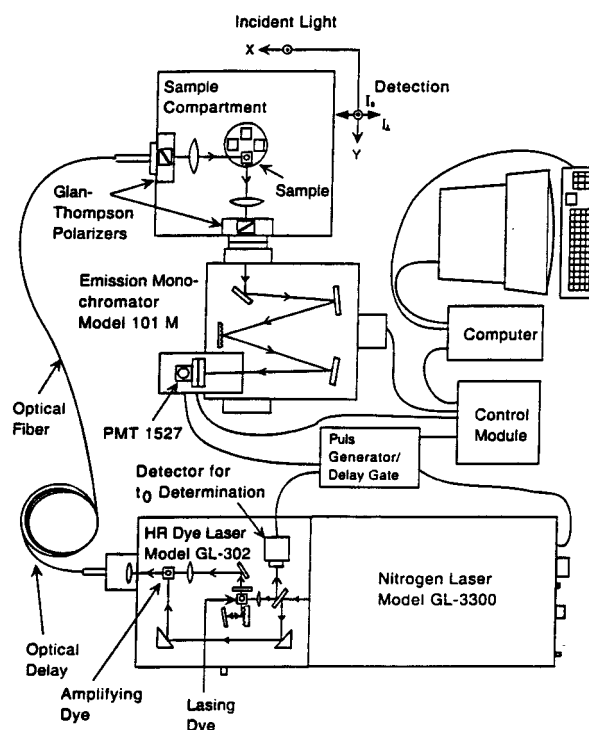
Figure 1. Schematic of the experimental set-up used for measurement of fluorescence anisotropy decay.

aromatics of the maltene (de-asphaltened crude oil) have also been examined. The comparison of maltene and asphaltene results is quite informative and further supports our asphaltene conclusions. In addition, the dependence of rotational correlation times versus concentration suggests the onset concentration of dimer or aggregate formation. These results are discussed with respect to known critical micelle concentrations of asphaltenes.

II. Experimental Section

For all solutions used herein, the optical densities were measured using a CARY 500 UV-visible-NIR spectrometer. The optical density is defined as the power of 10 reduction of incident light I_o vs transmitted light I ($I/I_o = 10^{-OD}$). For the collection of fluorescence spectra, we employed the PTI C-72 + A-720 fluorescence spectrometer using a 75-W Xe compact arc lamp source.

Figure 1 shows a schematic of the PTI C-72 system used for collection of the fluorescence time-dependent depolarization spectra. This system employs a PTI GL-3300 nitrogen laser source, along with a PTI GL-302 high-resolution dye laser with a fiber optic coupling to the measurement cell to excite the fluorescence. The excitation and emission light from the cell are oriented 90° from each other, with vertical polarization defined to be perpendicular to this plane. The wavelength of the PTI model 101 M emission monochromator is fixed, while two Glan-Thompson polarizers are used to select the polarizations. One polarizer is placed at the output of the fiber optic, immediately before the measurement cell, and the other polarizer is placed at the entrance to the emission monochromater. Fluorescence time-decay curves were collected for four polarizations; vertical on the source side, vertical on the emission side (v–v), vertical–horizontal (v–h), horizontal–vertical (h–v), and horizontal–horizontal (h–h).

The following procedure was used to acquire the time-decay spectra: the laser firing triggers a box-car delay gate, which then triggers a high-voltage pulse at known delay to the PMT.

Asphaltene Molecular Size and Structure

J. Phys. Chem. A, Vol. 103, No. 50, 1999 **11239**
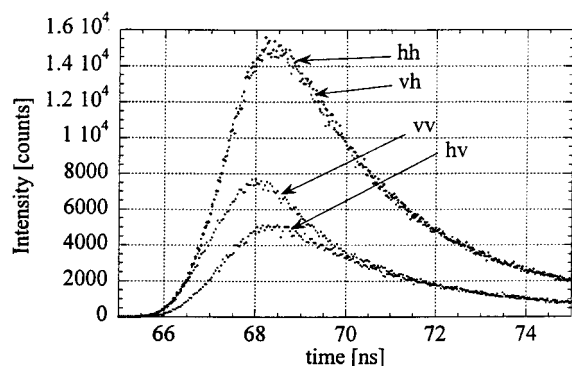
Figure 2. The four time-resolved fluorescence curves (with polarizations indicated) that are used to generate the anisotropy decay curve. The initially large difference between the v−v and v−h curves is due to anisotropy; the reduction of this difference with time is due to rotational diffusion.

Figure 3. Structure of the two dyes used for comparison with asphaltenes.

The short duration of the high-voltage pulse "turns on" the PMT for a short time interval. The integrated current over this time interval from the PMT is detected. The delay time is sequentially scanned over the desired time range, providing the fluorescence decay curve. The time resolution of the system is about 80 picoseconds.

A complete data set for one excitation and emission wavelength pair corresponds to acquisition of the four polarization combinations mentioned above. Typically, the total acquisition time for the four curves was 2 h. Reproducibility of signal levels was checked periodically during the acquisition time to validate the data. In addition, the v−h and h−h curves should overlay again, allowing for excellent quality control. The output of the fiber optic is randomized, so that selecting vertical or horizontal polarization for input into the cell gives the same power excitation. For both cases, a 90° rotation is required to align the source polarization vector with the horizontal acceptance polarization on the emission monochromater. Duplicate (or more) runs were performed for all wavelength pairs to assure precision. Typically, chi-square values of 1.2 or less were obtained for a good run. Changes in laser power during the run were associated with large values of chi-square.

Figure 2 shows typical data for a given wavelength pair, excitation at 530 nm and emission at 570 nm. The time-zero for the dye-laser pulse is at 67.6 ns. Typically, we used a wavelength shift of 40 nm between the excitation and emission to preclude any possibility of direct detection of scattered light. The h−h and v−h curves overlay, as expected. The large difference between the v−v and h−v curves at early times clearly shows a large anisotropy. This anisotropy decays at later times due to molecular rotation.

The v−h curve has a higher intensity than the v−v curve. This is due to the fact that horizontally and vertically polarized light have different transmission efficiencies through the emission channel of the instrument. This effect can be compensated for by introducing a calibration factor, which is usually denoted with a capital G and is defined as $G = I_{hv}/I_{hh}$; I_{ij} refers to excitation with i polarization and emission with j polarization. All experimental data sets were corrected by multiplication of G with I_{vh}. I_{vv}, then, refers to $I_{\parallel}$ and $I_{vh}G$ to $I_{\perp}$.

One crude oil sample we used was obtained from Kuwait (UG8). We also used a California heavy crude oil (Cal) to prepare a second asphaltene. There was no processing of the crude oils prior to the separation of asphaltenes; these are virgin crude oils. We prepared the *n*-heptane insoluble asphaltenes from this oil using procedures described elsewhere.[24] Briefly, a sample of the crude oil was mixed with 40 cc/g of *n*-heptane. The
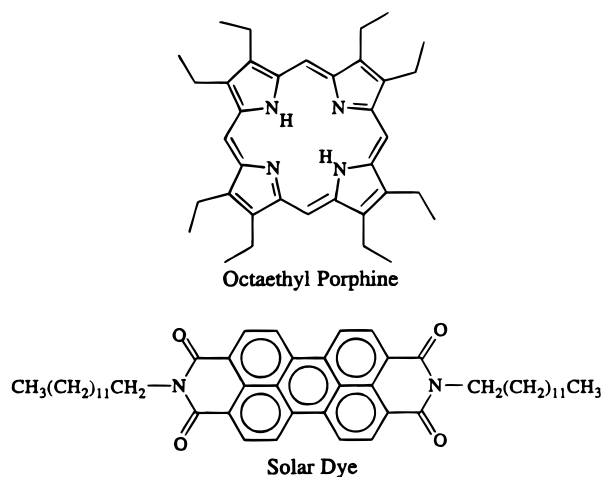
resulting solution was stirred in the dark for 24 h and then filtered using a 1.2-μm pore size nylon Schleicher and Schuell filter. The precipitate was washed with hot *n*-heptane until the solvent wash was colorless. The resulting powder was air-dried. To check for effects from trapped resin or other oil components, some of this asphaltene was then dissolved in toluene and reprecipitated again using a 40:1 volumetric ratio of *n*-heptane. After 24 h of stirring, the resulting precipitate was filtered and washed with hot *n*-heptane until the heptane wash was colorless. Furthermore, we note that the large heptane volume in this reprecipitation procedure was very light in color, indicating that our original asphaltene sample had little, if any, contamination of materials soluble in *n*-heptane. As will be shown, our original and reprecipitated asphaltene exhibited exactly the same effects in our data. There was no effect in our data from trapped resins and the like. A crude oil minus its asphaltenes is defined as "the maltenes" or sometimes referred to as deasphaltened crude oil. The resulting *n*-heptane solution of the maltenes was also used for analysis.

Optical densities of all solutions were kept below 0.2 OD to avoid complications from self-absorption (although the natural fluorescence red shift coupled with the decreasing absorption at longer wavelengths for all asphaltenes mitigates this effect). In addition, at concentrations in the range of 0.06 g/L and higher, the decay curves exhibited additional anisotropy decay components which may be associated with dimer formation. Consequently, we maintained asphaltene concentrations at or below 0.025 g/L for analysis. For instance, in Figure 2, the concentration is 0.006 g/L. All rotational correlation times were determined at room temperature (19 °C) and in toluene with a viscosity of 0.59 cP. Two dyes, obtained from Aldrich Chemicals, were also used in this study: octaethyl porphyin (OEP) and a solar dye, *N,N′*-ditridecyl-3,4,9,10-perylenetetracarboxylic diimide. Their structures are shown in Figure 3.

III. Theory

To develop the equations which describe the anisotropy decay of the fluorescence emission of fluorophores in solution, several different approaches were used.[30−36] The theory, mainly based on the work of Einstein[37,38] and Debye[39] on rotational diffusion by Brownian motion, was extended and presented in a final and complete version.[36]

In the following sections, we want to present two different approaches. The first treatment[32] approximates molecules as

spheres and is widely used to analyze experimental data;[40−46] the second is a complete description of the fluorescence anisotropy decay for asymmetric rotators.[36]

Spherical Model. In the following discussion, we will assume a spherical molecule rotating in a viscous medium subject to a sticking boundary condition.

The following definitions are used:[47]

$$D(t) = I_{\parallel}(t) - I_{\perp}(t) \tag{1}$$

$$S(t) = I_{\parallel}(t) + 2I_{\perp}(t) \tag{2}$$

and

$$r(t) = D(t)/S(t) \tag{3}$$

where $I_{\parallel}(t)$ and $I_{\perp}(t)$ denote detection of light linearly polarized parallel and perpendicular to the linearly polarized excitation, and $r(t)$ represents the anisotropy of the fluorescence emission.

We will assume an experimental setup as depicted in Figure 1. The exciting light is propagating in the negative x-direction and, its polarization is directed along the z-coordinate of a laboratory-fixed system. The fluorescence will propagate along the positive y-axis, and the polarization will be detected either in the z- or in the x-direction. The origin is placed conveniently at the position of the fluorophore. The transition dipole moment $\vec{\mu}$ shall have an arbitrary orientation with respect to the molecule axes. While the orientation of $\vec{\mu}$ stays constant in the molecular frame, it is time-dependent in the laboratory frame. The angles θ,ϕ define the orientation of $\vec{\mu}$ with respect to the laboratory frame. $W(\theta,\phi,t)$ shall now denote the probability that the vector $\vec{\mu}$ is oriented (θ,ϕ) at time t, and $G(\theta_0,\phi_0|\theta,\phi,t)$ the time evolution of the probability of $W(\theta,\phi,t)$ with $\vec{\mu}$ oriented in (θ_0,ϕ_0) at $t = 0$. The diffusion equation of the problem can now be written as

$$\frac{\partial W(\theta,\phi,t)}{\partial t} = D\nabla^2 W(\theta,\phi,t) \tag{4}$$

in which D is the diffusion constant of a sphere of volume V. Observing the transformation into spherical coordinates, the solution of the diffusion equation can be written in terms of its Green's function $G(\theta_0,\phi_0|\theta,\phi,t)$:

$$W(\theta,\phi,t) = \int_0^{2\pi} d\phi_0 \int_0^{\pi} \sin\theta_0 d\theta_0 W(\theta_0,\phi_0) G(\theta_0,\phi_0|\theta,\phi,t) \tag{5}$$

Since the probability for a molecule with a dipole $\vec{\mu}$ to absorb a photon with its electric vector $\hat{e}$ polarized in the z-direction is $|\vec{\mu}\cdot\hat{e}|^2 = \mu_z^2$, it is seen that the normalized initial distribution is[32]

$$W(\theta_0,\phi_0) = \frac{3}{4\pi}\cos^2\theta_0$$

$$= \frac{1}{4\pi}[1 + 2P_2(\cos\theta_o)] \tag{6}$$

where P_2 is the Legendre polynomial of the 2nd order. The Green's function can be expanded in terms of Legendre functions:[32]

$$G(\theta_0,\phi_0|\theta,\phi,t) = \sum_{l=0}^{\infty}\sum_{m=-l}^{l} c_{l,m}(t)Y^*_{l,m}(\theta_0,\phi_0)Y_{l,m}(\theta,\phi) \tag{7}$$

where only one expansion coefficient $c_{l,m}(t)$ is nonzero[32]

$$c_{l,m}(t) = e^{-6Dt} \tag{8}$$

The probability $W(\theta,\phi,t)$ is thereby calculated to

$$W(\theta,\phi,t) = \frac{1}{4\pi}[1 + 2c_{2,0}(t)P_2(\cos\theta)] \tag{9}$$

The orientation probability can now be used to calculate the intensity for the two different directions of polarization, which are given by[32]

$$I_{\parallel}(t) = \int\int \sin\theta d\theta d\phi \tilde{I}_{\parallel}(\theta,\phi,t)W(\theta,\phi,t)$$
$$I_{\perp}(t) = \int\int \sin\theta d\theta d\phi \tilde{I}_{\perp}(\theta,\phi,t)W(\theta,\phi,t) \tag{10a,b}$$

where $\tilde{I}_{\parallel}(\theta,\phi,t)$ and $\tilde{I}_{\perp}(\theta,\phi,t)$ are proportional to the fluorescence decay and the transition dipole vector component in the z- and x-direction, respectively. By solving the integrals, one obtains[32]

$$I_{\parallel}(t) = \frac{F(t)}{3}\left(1 + \frac{4}{5}c_{2,0}(t)\right)$$
$$I_{\perp}(t) = \frac{F(t)}{3}\left(1 - \frac{2}{5}c_{2,0}(t)\right) \tag{11a,b}$$

where $F(t)$ denotes the fluorescence decay. The anisotropy can now be calculated using eq 8:

$$r(t) = \frac{2}{5}e^{-6Dt} \tag{12}$$

Based on a method used by Einstein, an equation[48] was derived for the diffusion tensor **D**, which can be evaluated with the help of the drag tensor[49] $\boldsymbol{\beta}$. For a sphere, the tensor reduces to a scalar D

$$6D = \frac{kT}{V\eta} \tag{13}$$

(where η is the viscosity of the solvent) which makes it easy to relate the fluorescence anisotropy to the volume (V) of the sphere. The decay time of the anisotropy $\tau_{r,\text{sph}}$, the parameter of our experiment, can now be written as

$$\tau_{r,\text{sph}}^{-1} = \frac{kT}{V\eta} \tag{14}$$

Anisotropic Rotator. The more complex model of the anisotropic rotator can be treated completely in the operator formalism.[32,36] One starts by seeking a solution for the diffusion equation, which is given for the complete asymmetric body by

$$\frac{\partial W(\vec{\Omega},t)}{\partial t} = -(\vec{L}\cdot\mathbf{D}\cdot\vec{L})W(\vec{\Omega},t) \tag{15}$$

where $\vec{L}$ is the quantum mechanical angular momentum operator in units of $\hbar$, **D** is the diffusion tensor, and $W(\vec{\Omega},t)$ is, again, the probability that the vector of a molecular dipole transition $\vec{\mu}$ is oriented in the angle $\vec{\Omega}$ at time t. The angle $\vec{\Omega}$ refers to the orientation of a body-fixed coordinate system with respect to a laboratory system. This is solved using differential eq 15 by

Asphaltene Molecular Size and Structure

J. Phys. Chem. A, Vol. 103, No. 50, 1999 **11241**

the Green's function formalism:

$$W(\vec{\Omega},t) = \int_{\vec{\Omega}} W(\vec{\Omega}_0,t)G(\vec{\Omega}_0|\vec{\Omega}t)d\vec{\Omega}_0 \qquad (16)$$

where $W(\vec{\Omega}_0,t)$ is the distribution of the absorption dipoles at time $t = 0$.

By expanding the Green's function in terms of the eigenfunction of the asymmetric rotator, which again can be expanded in terms of the eigenfunction of the symmetric rotator for $l \leq 2$, and knowing that[36]

$$W(\vec{\Omega}_0,t) = P_{abs} \qquad (17)$$

where P_{abs} is the probability for the excitation of a molecule, it is possible to find a closed-form expression for $W(\vec{\Omega},t)$.[36]

Analogous to eq 10, one can use $W(\vec{\Omega},t)$ to obtain an expression for $I_{||}$ and $I_{\perp}$:

$$I_{||}(t) = \int_{\vec{\Omega}} P_{em}^{||} F(t) W(\vec{\Omega},t) d\vec{\Omega}$$

$$I_{\perp}(t) = \int_{\vec{\Omega}} P_{em}^{\perp} F(t) W(\vec{\Omega},t) d\vec{\Omega} \qquad (18a,b)$$

where $P_{em}^{||}$ and $P_{em}^{\perp}$ are the probabilities for the fluorescence emission polarized parallel and perpendicular to the incident light, respectively. The solutions to eq 18, when inserted into eqs 1−3, yield a five-exponential decay for the anisotropy $r(t)$ in the most general case:[36]

$$r(t) = \sum_{i=1}^{5} \alpha_i e^{-t/\tau_i} \qquad (19)$$

It is possible to reduce the number of lifetimes to three under the assumption of a body with a rotational symmetry.[32,50] In that case, the diagonalized diffusion tensor will have only two elements that are not equal, which we will label as $D_{||}$ and $D_{\perp}$. These two elements are governing the molecular relaxation due to Brownian motion parallel and perpendicular to the symmetry axis, respectively. The lifetimes of the anisotropy decay can be expressed as[32]

$$\tau_1^{-1} = 6D_{\perp}$$

$$\tau_2^{-1} = 5D_{\perp} + D_{||} \qquad (20)$$

$$\tau_3^{-1} = 2D_{\perp} + 4D_{||}$$

The diffusion coefficients were evaluated as[32]

$$D_{||} = \frac{3}{2} \frac{\rho(\rho - S)}{\rho^2 - 1} D$$

$$D_{\perp} = \frac{3}{2} \frac{\rho[(2\rho^2 - S) - \rho]}{\rho^4 - 1} D \qquad (21a,b)$$

where D is, again,

$$D = kT/6V\eta$$

the diffusion coefficient calculated for a sphere under the same conditions of volume, temperature, and viscosity as the ellipsoid,

TABLE 1: Anisotropy Decay Lifetimes as Appearing in Equation 20 as a Function of Aspect Ratios

$1/\rho$	$\tau_r/\tau_{r,\text{sph}}$	$\tau_1/\tau_{r,\text{sph}}$	$\tau_2/\tau_{r,\text{sph}}$	$\tau_3/\tau_{r,\text{sph}}$
2	1.41	1.13	1.17	1.30
4	2.25	1.84	1.90	2.10
6	3.09	2.65	2.71	2.93
8	3.94	3.47	3.54	3.77
10	4.79	4.30	4.38	4.62

ρ is the ratio of the longitudinal semiaxis to the equatorial semiaxis of the ellipsoid, and[32]

$$S = (\rho^2 - 1)^{-1/2} \ln[\rho + (\rho^2 - 1)^{1/2}] \qquad \rho > 1$$

$$S = (1 - \rho^2)^{-1/2} \arctan\left[\frac{(1 - \rho^2)^{-1/2}}{\rho}\right] \qquad \rho < 1$$

It is now verified that for an oblate rotator, both diffusion coefficients are approximately equal, and therefore all three τ_i's are approximately equal, too.[30] For different values of the aspect ratio, the three values of τ_i are shown in the last three columns of Table 1, confirming their near equivalency. The remaining anisotropy decay lifetime is[30]

$$\tau_r = \frac{2}{3} \frac{V\eta}{kT} \frac{\rho^2 - 1}{\rho(\rho - \{(1 - \rho^2)^{-1/2}\arctan[(1 - \rho^2)^{-1/2}/\rho]\})} \qquad (22)$$

The deviations of the anisotropy decay lifetimes for an oblate rotator τ_r from the anisotropy decay lifetimes of a spherical body $\tau_{r,\text{sph}}$ have been calculated for different aspect ratios.[32] In column 2 of Table 1, these deviations are listed.

For a given rotational correlation time, the ratio of the calculated major axis for an oblate spheroid to the calculated diameter for a sphere is $[(1/\rho)(\tau_{R,\text{sph}}/\tau_R)]^{1/3}$.

Data Fitting. To determine the rotational correlation time of the anisotropy decay, a difference curve $D(t)$ and a sum curve $S(t)$ according to eqs 1 and 2 were created and fitted by a least-squares method. Using eq 11, it can be shown that the sum curve corresponds to the fluorescence decay alone. For the fluorescence intensity decay (sum curve), a double exponential decay was used. Previous work has shown that the fluorescence intensity decay of asphaltenes is accurately represented using a double exponential decay.[27] Since the anisotropy decay is much faster than the fluorescence decay for our cases, then the difference curve is governed by the anisotropy decay. Consequently, the difference curve was fitted, in accordance to the theory, to a single exponential decay. A mean lifetime of the fluorescence intensity decay was calculated. Because the rotational decay constant is much faster ($\sim \times 10$) faster than the fluorescence decay, little error is introduced by this use of the mean fluorescence decay constant. Then, eq 3 was used with the mean fluorescence decay of the sum curve and the fluorescence decay of the difference curve to obtain $r(t)$. Substitution of $r(t)$ into eq 12, along with eqs 13 and 14, immediately gives $\tau_{r,\text{sph}}$. Use of the ratios $\tau_r/\tau_{r,\text{sph}}$ in column 2 of Table 2 allows the oblate spheroid τ_r to be obtained for the listed aspect ratios.

IV. Results and Discussion

Figure 4b shows the fluorescence emission spectrum of a dilute solution of UG8 asphaltene obtained with a 365-nm excitation. This spectrum represents the overlapping spectra of the many chromophores contained within the asphaltene. The spectral location of the fluorescence emission is related to the
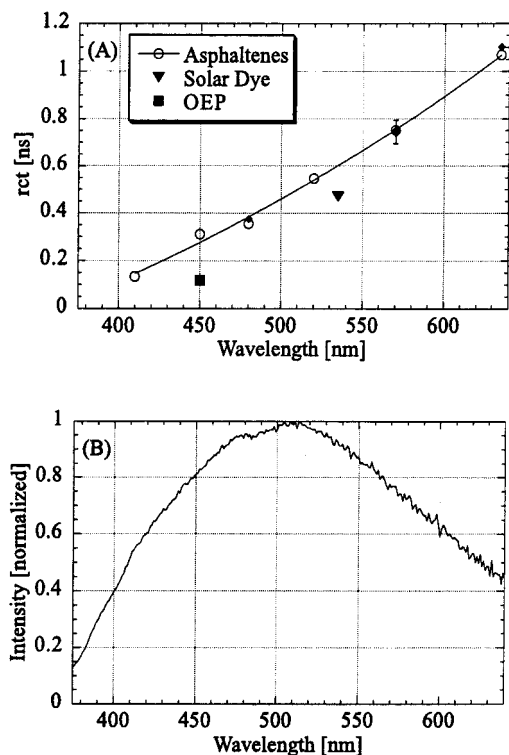
Figure 4. (a) The rotational correlation times of asphaltenes (and two dyes; square, triangle) vs emission wavelength. For each wavelength, the excitation wavelength is about 40 nm shorter than the emission wavelength. The superimposed open circles and diamonds are for repeat UG8 asphlaltene preparations. (b) The emission spectrum of the asphaltenes, showing their relevant spectral range.

TABLE 2: Ring Number and Fluorescence Emission Maxima for a Few Aromatic Hydrocarbons in *n*-Heptane

aromatic hydrocarbon	number of rings	HO−LU[a] excitation	emission maximum
benzene	1	265 nm	280 nm
naphthalene	2	300 nm	320 nm
anthracene	3	380 nm	390 nm
tetracene	4	475 nm	485 nm
pentacene	5	580 nm	590 nm

[a] HO−LU is highest occupied to lowest unoccupied.

size of the chromophore in accordance with the concepts of a quantum particle in a box. For example, Table 2 gives a listing of emission maxima for a few simple chromophores.

With changes in ring location and substitution, there is some change in spectral position of the fluorescence emission maximum; nevertheless, the wavelength of fluorescence emission does correlate with chromophore size. It is difficult to use the fluorescence emission spectrum to obtain an exact distribution of ring sizes because the optical absorption and emission constants are different for different chromophores. Nevertheless, these differences are mitigated because the somewhat smaller transition strength in smaller aromatics is offset by their larger quantum yields.[51] These two effects cancel to some degree. Estimating the range of size of asphaltene chromophores from the fluorescence emission spectrum is reasonable.[24]

Figure 4b shows that the asphaltene fluorescence emission is significant in the range of 400 to 650 nm. A previous comparison of fluorescence emission spectra of known standards with spectra of asphaltenes similar to Figure 4b yields an estimated range of fused rings to be 4−10.[24] This range in chromophore size is consistent with estimations from NMR[1−3,5,7] as well as determinations made by STM.[28]

By selection of excitation and emission wavelength, one can select a subset of chromophores. Long-wavelength excitation precludes excitation of small chromophores due to their large HO−LU (highest occupied to lowest unoccupied) gap. Correspondingly, with short-wavelength excitation, detection of fluorescence from large chromophores can be precluded by detecting short-wavelength emission; large chromophores emit long-wavelength fluorescence. The full range of chromophores is probed by tuning the excitation wavelength over the relevant spectral range while keeping a fixed wavelength difference between excitation and emission.

Figure 4a shows the rotational correlation time of asphaltenes as a function of the emission wavelength. These emission wavelengths correspond to the largest populations of asphaltene chromophores, as seen in Figure 4b. For each data point in Figure 4a, the excitation wavelengths are 40 nm shorter; that is, for each excitation wavelength λ_{ex} we used, we always used an emission wavelength λ_{em} where $\lambda_{em} = \lambda_{ex} + 40$ (all with units of nm). In addition, two known chromophores are also plotted in Figure 4a to provide a model-independent estimate of molecular size and molecular weight. Figure 4a is rich in results.

Absolute size of Asphaltene Molecules. There is a variation of a factor of 10 for the rotational correlation times for the most prominent asphaltene molecules. Using eq 14, one finds that the radius varies by about a factor of 2, independent of the shape of the molecules.

To convert from the rotational correlation time to molecular size, we list results presuming a sphere and presuming an oblate spheroid with an aspect ratio of 2 (or 1/2 more precisely) for the molecular geometry; there is not a great deal of difference in these two sets of results. The oblate spheroid is probably more accurate for asphaltene molecules as well as for the solar dye and OEP. If the molecular structures are actually oblate spheroids of an aspect ratio of 4, then all diameter entries in the last column would be increased by ∼9%. As shown by the Table 3 (and eq 14), there is not a large dependence of calculated diameters on moderate changes in molecular shape.

Table 3 shows the major axis diameters for the asphaltenes to be in the range of 10−20 Å. The STM results quoted a mean value of the aromatic component of asphaltenes to be 10 Å in diameter. The fluorescence depolarization technique is sensitive to the size of the entire molecule, while the STM method is sensitive to the size of the aromatic portion only, which is roughly 40% of the molecule. Both techniques yield comparable and small sizes for the asphaltene molecules.

Table 4 compares the rotational correlation times of two asphaltenes, one from Kuwait (UG8) and one from California (Cal). The results are consistent, showing the same trends; first, the rotational correlation times are small, and second, the rotational correlation times vary by a factor of 10 over the relevant spectral range for asphaltenes. The salient feature of Table 4 is that our results are general for asphaltenes. The topic of a detailed comparison of different asphaltenes will be the subject of a future paper.

In addition, we have used the UG8 asphaltene in a series of studies including nitrogen XANES,[5,11] sulfur XANES,[5,9] optical absorption spectroscopy,[6,25] and fluorescence emission spectroscopy;[6,27] UG8 asphaltene has obeyed the same systematic trends exhibited by the ten asphaltenes (from three continents) that we have used in our studies. UG8 asphaltene is a representative asphaltene.

Comparison of Dyes to Previous Work. Table 3 also lists the diameters for two dyes. Previously, the size of a metallo-

TABLE 3: Fluorescence Absorption and Emission Wavelengths, Rotational Correlation Times, Fluorescence Anisotropy, and the Molecular Diameter (Major Axis for Oblate Spheroid) for UG8 Asphaltene and Two Dyes

sample	λex (nm)	λem (nm)	τ (ns)	anisotropy	diameter (Å) sphere	diameter (Å) oblt. sph. $\rho = 1/2$
asphaltene	365	410	0.1340	0.5907	12.02	13.50
UG8	406	450	0.3115	0.3389	15.92	17.89
	440	480	0.3561	0.3365	16.65	18.70
	480	520	0.5464	0.2623	19.20	21.57
	530	570	0.7518	0.2737	21.35	23.9
	595	635	1.0688	0.2963	24.01	26.98
solar dye	480	535	0.4704	0.3111	18.26	20.52
OEP	406	450	0.1194	0.4248	11.56	12.99

TABLE 4: Rotational Correlation Times for Two Asphaltenes vs Excitation and Emission Wavelengths

λex (nm)	λem (nm)	τ (ns) Cal asph.	τ (ns) Ug8 asph.
365	410	0.0776	0.1340
406	450	0.2087	0.3115
440	480	0.2419	0.3561
480	520	0.4071	0.5464
530	570	0.6264	0.7518
595	635	0.9058	1.0688

OEP was determined by measuring the rotational correlation time using the very different technique, perturbed angular correlation of gamma rays (PAC).[52] (The central metal in the porphyrin has no impact on the diameter of the porphyrin.) In that work, a spherical model was used, and a diameter of 11.6 Å was found for OEP. Here, using the same spherical model (eq 14), we obtain a diameter of 11.6 Å for OEP. The agreement is exceptional, especially considering that there are no adjustable parameters in either case. We also note that the previous study showed that the addition of tetraphenyl substitution at the meso sites (methine bridges) dramatically increased the rotational correlation time,[52] perhaps in part because the phenyl rings are perpendicular to the porphyrin rings.[53] Furthermore, this value agrees favorably with X-ray structures of porphyrins.[53]

Asphaltene Molecular Weight. To obtain a good estimation of the molecular weight with a model-independent analysis, we used as standards two known molecules with a disk shape, similar to that expected for asphaltenes. Figure 3 shows the structures of these two molecules. The rotational correlation time of the porphyrin OEP is at the lower limit for the asphaltenes. The molecular weight of the porphyrin is 535 amu, giving the lower-value estimation for the asphaltene molecular weights of 500 amu. The rotational correlation time of the solar dye is located roughly at the mean correlation time of the asphaltenes. The molecular weight of the solar dye is 755 amu, giving an estimate of 750 amu for the mean asphaltene molecular weight. Extrapolating the size–molecular weight relation, we estimate the maximum molecular weight of the asphaltenes to be about 1000 amu.

Number of Chromophores per Asphaltene Molecule. Figure 4 also shows that there is a monotonic, order-of-magnitude increase in the rotational correlation time across the asphaltene spectral range; that is, there is a strong correlation between the size of the asphaltene chromophore, given by the emission wavelength and the size of the molecule, given by the rotational correlation time. This correlation requires that asphaltene molecules have only one or two chromophores per molecule. If an asphaltene molecule possessed, say 10 chromophores per molecule, then there would be no correlation between chromophore size and molecular size. A small chromophore attached to a large molecule would exhibit the slow rotational correlation time of the entire, large molecule. The

fact that we measure fast rotation for small chromophores and a factor of 10 slower rotation for large chromophores means that these individual chromophores are an appreciable fraction of the asphaltene molecule. Thus, asphaltene molecules possess one or two chromophores per molecule, on average.

Limiting the number of chromophores per asphaltene molecule also limits the molecular weight. If an asphaltene molecule contains a single seven fused-ring system with 40% of the carbon being aromatic, then the molecular weight of the molecule cannot deviate too much from 750 amu and is far smaller than the estimation of several thousand amu that is encountered, for example, from VPO or GPC. Our two results, the absolute rotational correlation rates and the relative dependence of the correlation rates on emission wavelength, are independent. Both of these results support the contention that asphaltene molecules have molecular weights in the range of 750 amu. These measurements are made with asphaltene solutions that are extremely dilute. Higher concentrations used for some other measurements of molecular weights undoubtedly yield higher values due to formation of asphaltene aggregates or micelles. The controversy over asphaltene molecular weights should now subside.

Maltenes. It is instructive to compare the asphaltene rotational correlation times with those chromophores in maltenes of comparable spectral properties. Figure 5a shows the maltene rotational correlation times along with the asphaltene correlation times. Figure 5b shows that the fluorescence emission spectrum of the UG8 maltenes peaks at much shorter wavelengths, corresponding to a smaller mean size of maltene chromophores. The high emission intensity in the 390–410-nm range corresponds to the large population of roughly 3–4 ring chromophores. (The 365-nm source wavelength is of too low an energy to excite one- and two-ring chromophores.) Thus, as expected, the bulk of chromophores found in maltenes possess fewer rings than those of asphaltenes. Nevertheless, one can perform measurements on the largest maltene chromophores, which are comparable to those of asphaltenes.

Figure 5 shows that for any given emission wavelength, the maltene rotational correlation times are somewhat smaller than those of the asphaltenes. This means that the maltene molecules of particular spectral properties are smaller than those of the asphaltene, as expected. In other words, if two large molecules of somewhat different size possess the same emission wavelength, the larger of the two would have a stronger tendency to be in the asphaltene fraction and the smaller one in the maltene. In addition, the maltenes exhibit the same correlation of molecular size with chromophore size. As with the asphaltenes, this indicates that the maltene molecules only have one or two chromophores per molecule. This result is expected even for the heaviest fraction of the maltenes, the resins. This figure also implies a rather continuous transition in molecular size in going
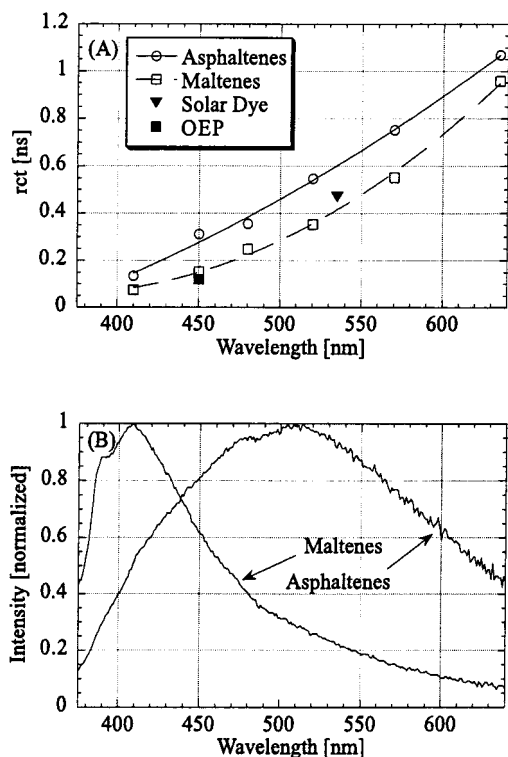
Figure 5. (a) The rotational correlation times of asphaltenes, maltenes, and two dyes vs emission wavelength. For each wavelength, the excitation wavelength is about 40 nm shorter than the emission wavelength. (b) The emission spectrum of UG8 asphaltene and maltene.

from resins to asphaltenes. There does not appear to be a sudden transition in molecular structural properties.

Aggregation. An important issue associated with molecular size and weight determination of asphaltenes is the issue of aggregation. Asphaltenes are known to form micelles at fairly low concentrations, for example, at ~0.5 g/L for vacuum resid in pyridine.[14,18] Of course, some degree of complex formation could occur at even lower concentrations for this polydisperse material. Furthermore, vacuum resid asphaltenes in pyridine could behave differently than virgin crude oil asphatenes in toluene. We used asphaltene solutions at concentrations in the range of 0.01 g/L and found no change in results at higher dilution (except signal-to-noise degraded). At concentrations higher than about 0.06 g/L, we found that our anisotropy decay curve was no longer represented by a single exponential, as it is for lower concentrations. Systematic variations in both the residuals and growth of the chi-square values illustrated this point. Also, with these fits at higher concentrations, the calculated value of the rotational correlation time increased. We believe that we are observing the onset of molecular aggregation (presumably dimer formation) at 0.06 g/L. For such a polydisperse system, the presumption is that dimer formation would occur at a lower concentration than micelle formation, so our results are consistent with the previous CMC results.[18] Such a low concentration for the onset of molecular aggregation would help explain why many techniques that require much higher concentrations, (>0.1 g/L) would yield asphaltene molecular weights that are too high. The experimental difficulty of optical opacity precluded our going to yet higher asphaltene concentrations.

The low concentrations we used prevent intermolecular electronic energy transfer. When excited states have additional deexcitation pathways leading to quenching and energy transfer, with subsequent fluorescence from the second chromophore,

three effects are noted for the originally excited chromophore: a reduction of the fluorescence lifetime, a reduction of the quantum yield, and a red shift in the fluorescence spectrum.[6] We have measured all of these effects induced by electronic energy transfer in solutions with high concentrations of crude oils and asphaltenes.[6,51,54,55] In order to determine whether asphaltenes exhibit intramolecular energy transfer, a careful study was done to determine if asphaltene fluorescence lifetimes are reduced below those obtained for maltenes.[27] The measured lifetimes of these two components were essentially the same, indicating that there is no significant intramolecular energy transfer in asphaltenes.[27] The most likely reason is that the asphaltene molecules possess, for the most part, only one chromophore per molecule, precluding intramolecular energy transfer. In addition, those asphaltenes with two chromophores may have restrictive alkane linkages, preventing the optimal geometry for energy transfer. In any event, excitation of the largest chromophore in the molecule cannot result in energy transfer.

V. Conclusions

The asphaltene rotational correlation times were measured, and corresponding asphaltene molecular diameters were in the range of 10−20 Å. Using known chromophores, asphaltene molecular weights are estimated to be in the range of 500−1000 amu. Furthermore, the strong correlation between chromophore size and asphaltene molecular size indicates that asphaltenes possess 1 or 2 chromophores per molecule. This finding independently confirms the low asphaltene molecular weights reported here. Our results are consistent with previously reported STM results and mass spectroscopy results for petroleum asphaltenes. The confluence of evidence from three very different techniques should end the controversy over the values of asphaltene molecular weights. Analysis of corresponding maltene data implies only subtle molecular structure changes in going from the largest maltene molecules to the asphaltenes. Our data suggest that asphaltene molecular aggregation occurs at low concentrations, 0.06 g/L, helping to explain why larger molecular weights are reported for techniques that require high concentrations.

References and Notes

(1) *Bitumens, Asphalts, and Tar Sands*; Chilingarian, G. V., Yen, T. F., Eds.; Elsevier Scientific Publishing Co.: New York, 1978.

(2) Speight, J. G. *The Chemistry and Technology of Petroleum*; Marcel Dekker: New York, 1980.

(3) Tissot, B. P.; Welte, D. H. *Petroleum Formation and Occurrence*; Springer-Verlag: Berlin, 1984.

(4) *Chemistry of Asphaltenes*; Bunger, J. W., Li, N. C., Eds.; American Chemical Society: Washington, DC, 1984.

(5) *Asphaltenes, Fundamentals and Applications*; Sheu, E. Y.; Mullins, O. C., Eds.; Plenum Press: New York, 1995.

(6) *Structures and Dynamics of Asphaltenes*; Mullins, O. C., Sheu, E. Y., Eds.; Plenum Press: New York, 1998.

(7) Calemma, V.; Iwanski, P.; Nali, M.; Scotti, R.; Montanari, L. *Energy Fuels* **1995**, *9*, 225.

(8) George, G. N.; Gorbaty, M. L. *J. Amer. Chem. Soc.* **1989**, *111*, 3182.

(9) Waldo, G. S.; Mullins, O. C.; Penner-Hahn, J. E.; Cramer, S. P. *Fuel* **1992**, *71*, 53.

(10) Kelemen, S. R.; George, G. N.; Gorbaty, M. L. *Fuel* **1990**, *69*, 939.

(11) Mitra-Kirtley, S.; Mullins, O. C.; van Elp, J.; George, S. J.; Chen, J.; Cramer, S. P. *J. Am. Chem. Soc.* **1993**, *115*, 252.

(12) Pollack, S. S.; Yen, T. F. *Anal. Chem.* **1970**, *42*, 623.

(13) Sheu, E. Y. *Phys. Rev. A* **1992**, *45*, 2428.

(14) Sheu, E. Y. In ref. 5.

(15) Ravey, J. C.; Decouret, G.; Espinat, D. *Fuel* **1988**, *67*, 1560.

(16) Anisimov, M. A.; Yudin, I. K.; Nikitin, V.; Nikolaenko, G.; Chernoustan, A.; Toulhoat, H.; Frot, D.; Briolant, Y. *J. Phys. Chem.* **1995**, *99*, 9576.

(17) Speight, J. G. *Am. Chem. Soc., Div. Pet. Chem. Preprints* **1981**, *26*, 825.

(18) Sheu, E. Y.; De Tar, M. M.; Storm, D. A.; DeCanio, S. J. *Fuel* **1992**, *71*, 299.

(19) Anderson, S. I.; Speight, J. G. *Fuel* **1993**, *72*, 1343.

(20) Payzant, J. D.; Lown, E. M.; Strausz, O. P. *Energy Fuels* **1991**, *5*, 445.

(21) Boduszynski, M. M. Chapter 7 in ref 4.

(22) Boduszynski, M. M. *Energy Fuels* **1988**, *2*, 597.

(23) Miller, J. T.; Fisher, R. B.; Thiyagarajan, P.; Winans, R. E.; Hunt, J. E. *Energy Fuels* **1998**, *12*, 1290.

(24) Mullins, O. C. Chapter 2 in ref 6.

(25) Mullins, O. C.; Zhu, Y. *Appl. Spectros.* **1992**, *46*, 354.

(26) Mullins, O. C.; Mitra-Kirtley, S.; Zhu, Y. *Appl. Spectros.* **1992**, *46*, 1405.

(27) Ralston, C. Y.; Mitra-Kirtley, S.; Mullins, O. C. *Energy Fuels* **1996**, *10*, 623.

(28) Zajac, G. W.; Sethi, N. K.; Joseph, J. T. *Scan. Micros.* **1994**, *8*, 463.

(29) Strausz, O. P.; Mojelsky, T. W.; Lown, E. M. *Fuel* **1992**, *71*, 1355.

(30) Perrin, F. *J. Phys. Radium* **1926**, *7*, 390.

(31) Perrin, F. *J. Phys. Radium* **1936**, *7*, 1.

(32) Tao, T. *Biopolymers* **1962**, *8*, 607.

(33) Weber, G. *J. Chem. Phys.* **1971**, *55*, 2399.

(34) Belford, G. G.; Belford, R. L.; Weber, G. *Proc. Natl. Acad. Sci. U.S.A.* **1972**, *69*, 1392.

(35) Ehrenberg, M.; Rigler, R. *Chem. Phys. Lett.* **1972**, *14*, 539.

(36) Chuang, T. J.; Eisenthal, K. B. *J. Chem. Phys.* **1972**, *57*, 5094.

(37) Einstein, A. *Ann. Phys.* **1905**, *17*, 549.

(38) Einstein, A. *Ann. Phys.* **1906**, *19*, 371.

(39) Debye, P. *Polar Molecules*; Dover Publications: Mineola, NY, 1929; Chapter 5.

(40) Rice, S. A.; Kenney-Wallace, G. A. *Chem. Phys.* **1980**, *47*, 161.

(41) Tsunomori, F.; Ushiki, H. *Bull. Chem. Soc. Jpn.* **1996**, *69*, 1849.

(42) Cross, A. J.; Fleming, G. R. *Biophys. J.* **1984**, *46*, 45.

(43) Tsunomori, F.; Ushiki, H. *Polym. J.* **1996**, *28*, 576.

(44) Sasaki, T.; Hirota, H.; Yamamoto, M.; Nishijima, Y. *Bull. Chem. Soc. Jpn.* **1986**, *60*, 1165.

(45) Horinaka, J.; Ono, K.; Yamamoto, M. *Polym. J.* **1985**, *14*, 433.

(46) Chang, M. C.; Courtney, S. H.; Cross, A. J.; Gulotty, R. J.; Petrich, J. W.; Fleming, G. R. *Analyt. Instr.* **1985**, *14*, 433.

(47) Wahl, P. In *Biochemical Fluorescence: Concepts*; Chen, R. F., Edelhoch, H., Eds.; Marcel Dekker, Inc.: New York, 1975; Vols. 1, 2, Chapter 1.

(48) Favro, L. D. *Phys. Rev.* **1960**, *119*, 53.

(49) *Noise and Stochastic Processes*; Wax, N., Ed.; Dover Publications: New York, 1954.

(50) Small, E. W.; Isenberg, I. *Biopolymers* **1977**, *16*, 1907.

(51) Ralston, C. Y.; Wu, X.; Mullins, O. C. *Appl. Spectrosc.* **1996**, *50*, 1563.

(52) Mullins, O. C.; Kaplan, M. *J. Chem. Phys.* **1983**, *79*, 4475.

(53) Scheidt, W. R. In *The Porphyrins*; Dolphin, D.; Ed.; Acedemic Press: New York, 1978; Vol. 3, Chapter 10.

(54) Downare, T. D.; Mullins, O. C. *Appl. Spectrsoc.* **1995**, *49*, 754. Also published in *Selected Papers on Laser Beam Diagnostics*; Hindy, R. N., Hunt, J. H., Eds.; SPIE Milestones Series Vol. MS 126; SPIE Optical Engineering Press: Washington, 1996.

(55) Wang, X.; Mullins, O. C. *Appl. Spectrosc.* **1994**, *48*, 977.